INORGANIC CHEMISTRY
FRONTIERS

RESEARCH ARTICLE

View Article Online
View Journal | View Issue

Cite this: *Inorg. Chem. Front.*, 2022, **9**, 2173

$Ln_3@C_{80}^+$ (Ln = lanthanide): a new class of stable metallofullerene cations with multicenter metal–metal bonding in the sub-nanometer confined space†

Yuhang Jiang, Zisheng Li, Yabei Wu and Zhiyong Wang *

Among the large number of members in the metallofullerene family, the nitride clusterfullerene $M_3N@C_{80}$ (M = trivalent metal) is a special one with extraordinarily high stability. It is generally thought that the molecule would be unstable without the nitrogen ion N^{3-} in the center of the M_3 moiety, because N^{3-} can compensate for the Coulomb repulsion between the metal ions M^{3+}. Indeed, the tri-metallofullerenes $Ln_3@C_{80}$ (Ln = trivalent lanthanide) are missing in the family of metallofullerenes to date. In this paper, we provide new insights into the stability of $Ln_3@C_{80}$ by a combined experimental and theoretical study. Density functional calculations demonstrate that $Ln_3@C_{80}$ are thermodynamically stable molecules. However, their small HOMO–LUMO gaps can induce severe kinetic instability. Meanwhile, $Ln_3@C_{80}$ has the smallest ionization energy among the metallofullerene molecules reported so far. Experimental and theoretical studies prove that the $Ln_3@C_{80}$ molecules can be greatly stabilized by chemical oxidation, because the $Ln_3@C_{80}^+$ cation has a large HOMO–LUMO gap comparable to that of $Ln_3N@C_{80}$. Furthermore, $Ln_3@C_{80}^+$ and $Ln_3N@C_{80}$ have similar molecular geometries and electronic structures. There is a three-center two-electron σ bond in the center of the Ln_3 cluster in $Ln_3@C_{80}^+$. This special metal–metal bond significantly compensates for the electrostatic repulsion between the Ln ions and thus stabilizes the cation $Ln_3@C_{80}^+$. In previous studies, there are very few examples of metallofullerene cations, because most of the metallofullerene cations are highly unstable. This study provides a strategy for obtaining a new class of stable metallofullerene cations, which can be used to construct a variety of novel ionic compounds $Ln_3@C_{80}^+X^-$.

Received 7th January 2022,
Accepted 13th March 2022

DOI: 10.1039/d2qi00051b

rsc.li/frontiers-inorganic

1 Introduction

As unique core–shell structured clusters, endohedral metallofullerenes (EMFs) have been intensively investigated due to their tunable physicochemical properties. In recent decades, a variety of metallofullerenes, such as mono-metallofullerenes ($M@C_{2n}$), di-metallofullerenes ($M_2@C_{2n}$) and endohedral clusterfullerenes ($M_xA_y@C_{2n}$ (A = nonmetal element)), have been synthesized and theoretically investigated.[1–4] Among these metallofullerenes, the C_{80}-containing ones are attractive compounds, not only because of the high symmetry of I_h-C_{80} but also for its ability to accommodate two metal atoms or a mixed metal/nonmetal cluster.[5–13]

On one hand, the outer C_{80} fullerene cage provides a sub-nanometer confined space to capture and stabilize the originally unstable cluster with novel chemical bonding types. For instance, a two-center one-electron metal–metal bond has been discovered in $M_2@C_{80}$ (M = Y or lanthanides).[14–17] The radical bridge between the two metals is well-protected by the fullerene cage, and it leads to strong magnetic exchange coupling between lanthanide ions in $Ln_2@C_{80}$.[18] On the other hand, electron transfer from the encapsulated metal species to the outer C_{80} cage results in a strong Coulomb repulsion between the highly charged metal ions. Although the fullerene cage restricts the dissociation of the encapsulated metal cluster, the metal atoms still tend to be as far from each other as possible. When three or more metal atoms are encapsulated in the fullerene cage, introducing one or more non-metal atoms is usually necessary to partially compensate for the Coulomb repulsion between the metal atoms. One typical example is the nitride clusterfullerene $M_3N@C_{80}$, which can be described as $(M^{3+})_3N^{3-}@C_{80}^{6-}$.[19]

In contrast to the well-studied nitride clusterfullerene $M_3N@C_{80}$ (M = trivalent metal), much less is known about the

Key Laboratory of Advanced Light Conversion Materials and Biophotonics, Department of Chemistry, Renmin University of China, Beijing 100872, PR China. E-mail: zhiyongwang@ruc.edu.cn

†Electronic supplementary information (ESI) available: Additional calculation results and molecular coordinates. See DOI: https://doi.org/10.1039/d2qi00051b

corresponding tri-metallofullerene $M_3@C_{80}$. Although the synthesis of Tb_3C_{80} has been reported previously,[20] it is not clear whether Tb_3C_{80} is the conventional metallofullerene $Tb_3@C_{80}$ or carbide clusterfullerene $Tb_3C_2@C_{78}$. A theoretical study on $Y_3@C_{80}$ suggests that $Y_3@C_{80}$ is more stable than $Y_3C_2@C_{78}$ and that $Y_3@C_{80}$ mimics $Y_3N@C_{80}$ with a pseudoatom instead of the nitrogen atom in the center of the molecule.[21] Shi and coworkers have reported the crystal structure characterization of $Sm_3@I_h$-C_{80}.[22] It should be noted that the oxidation state of Sm in the metallofullerene is +2, which is different from that of the metals in $M_3N@C_{80}$. Thus, the Sm element cannot form a nitride clusterfullerene. Other reports on metallofullerenes containing three metal atoms include the synthesis of Er_3C_{74} [23] and Dy_3C_{98}.[24] The bonding character of the Er_3 cluster in C_{74} has been studied theoretically.[25] The metallofullerenes mentioned above were produced by vaporizing metal/graphite composite rods with a Krätschmer–Huffman fullerene generator. Tri-metallofullerenes with larger sizes were observed in the gas phase by the method of laser ablation.[26–29]

For the lanthanide elements that can form nitride clusterfullerenes (such as Gd, Dy, Er, Tm, Lu, *etc.*), it is still an open question whether they can form tri-metallofullerenes $Ln_3@C_{80}$. If the formation of $Ln_3@C_{80}$ is possible, several questions would be raised: (i) which lanthanide elements prefer to form stable tri-metallofullerenes $Ln_3@C_{80}$? (ii) How the electronic and chemical properties of $Ln_3@C_{80}$ are affected by different lanthanide metal atoms? (iii) How to stabilize or capture such $Ln_3@C_{80}$ molecules? To address these issues, we conducted a theoretical investigation on $Ln_3@C_{80}$ (Ln = La, Nd, Gd, Tb, Dy, Ho, Er, Tm, Lu) by employing density functional theory (DFT) calculations. The molecular structures, stabilities, electronic properties and bonding features of $Ln_3@C_{80}$ were investigated. DFT calculations reveal that the $Ln_3@C_{80}$ compounds have small ionization energies and that they are prone to lose an electron to form a stable cation. We have obtained the cation $Ln_3@C_{80}^+$ in experiments through the chemical oxidation of $Ln_3@C_{80}$. In the research field of metallofullerenes, most studies were conducted on neutral metallofullerene molecules. The knowledge on metallofullerene cations is very limited, because most of them are not stable. The only example of a stable metallofullerene cation reported so far is $[Li@C_{60}]^+$. It can be used to construct a variety of ionic compounds $[Li@C_{60}]^+X^-$ (X = $SbCl_6$, PF_6, *etc.*), which have unique structures and fascinating properties.[30–33] The tri-metallofullerenes $Ln_3@C_{80}^+$ reported in this paper represent a new class of stable metallofullerene cations with unique metal–metal bonding features.

2 Methods

2.1 Computational details

Previous studies have demonstrated that density functional calculations using PBE[34] and PBE0 [35] functionals can give reasonable results on the geometries and energies of metallofullerenes.[9,15,21,36–38] In this study, the geometrical structures of $Ln_3@C_{80}$ (Ln = La, Nd, Gd, Tb, Dy, Ho, Er, Tm, Lu) and their cations were optimized using the PBE and PBE0 functionals. It should be noted that some of these molecules contain a partially-filled 4f-shell. It is difficult to treat such electronic configurations by single-determinant DFT calculations. Considering that the 4f electrons of lanthanide atoms are usually not involved in the chemical bonding of metallofullerenes, we employed ECP*n*MWB (*n* is the number of core electrons) with 4f-in-core effective core potentials and the corresponding valence basis sets for the lanthanide atoms. In a recent work by Popov and coworkers,[39] the results of DFT calculations on $Dy_3C_2@C_{80}$ with a similar 4f-in-core treatment are consistent with the experimental results, confirming the reliability of such a calculation method.

For geometry optimization, the 6-31G(d) basis set[40] was used for the carbon atom. For single-point energy calculations, the extended basis set 6-311G(d)[41] was used instead. Vibrational frequency analyses were performed on the optimized structures to ensure that they are local minima on the energy potential surface. To investigate the bonding nature of the $Ln_3@I_h$-C_{80} molecules, the Mayer bond order (MBO),[42] multicenter bond order (MCBO)[43] and electron localization function (ELF)[44] were examined using the MULTIWFN 3.7 program.[45] All the DFT calculations in this study were carried out using the Gaussian 16 Rev. A03 package.[46] The calculated results were visualized using visual molecular dynamics (VMD).[47]

2.2 Experimental section

Trimetallofullerene $Tm_3@C_{80}$ was prepared by using the arc-discharge method. A hollow graphite rod filled with a mixture of Tm_2O_3 and graphite powder (molar ratio of Tm : C = 1 : 15) was used as the anode, and a pure graphite rod was used as the cathode. The arc discharge was performed at a current of 100 A under a He atmosphere (200 Torr). The arc-produced raw soot was oxidized by $AgSbF_6$ in dichloromethane (DCM) in a nitrogen-filled glove box for 24 h. After the oxidation reaction, the solution was separated from the insoluble soot residue by centrifugation. The resulting dark-brown solution was filtered through a membrane filter (pore diameter = 0.22 μm), and it was vacuum-evaporated to remove the solvent. Then the solid was dissolved in a mixed solvent of toluene and acetonitrile (1 : 1). The composition of the solution was characterized by using laser desorption ionization time of flight (LDI-TOF) mass spectrometry (AB Sciex 5800 mass spectrometer).

3 Results and discussion

3.1 Stability of $Ln@C_{80}$

For C_{80}-based clusterfullerenes containing three metal atoms, such as $M_3N@C_{80}$,[19] $M_3C_2@C_{80}$,[39,48] $Sc_3CH@C_{80}$ [10] and $Ti_3C_3@C_{80}$,[49] it is generally accepted that the encapsulated cluster transfers six electrons to the fullerene cage. On the other hand, for trimetallofullerenes without any non-metal mediator, such as $Y_3@C_{80}$ [21] and $Er_3@C_{74}$,[25] the inner metal atoms are also thought to donate six electrons in total to the

outer cage. Therefore, the stability of these metallofullerenes is related to the stability of the fullerene cage in the hexaanionic state C_{2n}^{6-}.

In a previous study by Popov and coworkers, the relative energy of C_{80}^{6-} isomers has been calculated theoretically.[36] In order to determine which isomer is most preferable in energy for encapsulation of three lanthanide atoms to form $Ln_3@C_{80}$, we used the nine lowest energy isomers of C_{80}^{6-} as the candidates for the host fullerene cage. Three lanthanide atoms were encapsulated in these fullerene cages to form nine isomers of $Ln_3@C_{80}$. The calculated relative energies based on PBE and PBE0 functionals are summarized in Table S1.† It can be found that $Ln_3@C_{80}$ based on I_h and D_{5h} cage structures are the two lowest energy isomers. In this work, $Tm_3@C_{80}$ was selected as a representative compound for further discussion. The relative energies and HOMO–LUMO gaps of $Tm_3@C_{80}$ isomers are listed in Table 1. It is found that the most stable isomer of $Tm_3@C_{80}$ is $Tm_3@I_h$ (31 924)-C_{80}, which is more stable than the others by at least 13 kcal mol^{-1}. The second most stable isomer is $Tm_3@D_{5h}$ (31 923)-C_{80}. The stability order of $Tm_3@C_{80}$ is similar to that of $Tm_3N@C_{80}$.[50] Further theoretical studies in this work were conducted on the most stable isomer, *i.e.* $Tm_3@I_h$-C_{80}.

It is known that some metal carbide clusterfullerenes $M_xC_y@C_{2n}$ are lower in energy as compared with their metallofullerene form $M_x@C_{2n+y}$.[48,51–54] To compare the stability of $Tm_3@I_h$-C_{80} and $Tm_3C_2@C_{78}$, we also performed calculations on $Tm_3C_2@C_{78}$. The calculated results reveal that $Tm_3C_2@C_{78}$ has a higher energy than $Tm_3@I_h$-C_{80} (see Table S2†). Therefore, it can be concluded that $Tm_3@I_h$-C_{80} is thermodynamically more stable than its carbide form.

In previous studies, the stability of the nitride clusterfullerene $M_3N@C_{80}$ for various metals has been investigated.[36,55,56] It has been found that some lanthanide atoms such as La and Nd are too large to be encapsulated in the I_h-C_{80} fullerene cage. For the metallofullerene $Ln_3@I_h$-C_{80}, the size of the encapsulated atom may have a similar effect on the stability of the metallofullerene. In this work, the stability of $Ln_3@I_h$-C_{80} for various lanthanide elements was evaluated by calculating the following energetic parameters. The first one is the formation energy (ΔE_f), which was calculated based on the hypothetical reaction (1). In addition, we also calculated the binding energy (ΔE_b) and the encapsulation energy (ΔE_{encap}) based on hypothetical reactions (2) and (3). Previous studies have demonstrated that large binding energy and encapsulation energy values suggest high stability of metallofullerenes.[57] Meanwhile, the cluster formation energy ($\Delta E_{cluster}$) based on reaction (4) could be obtained by subtracting the binding energies (ΔE_b) from the encapsulation energies (ΔE_{encap}).

$$3M + 80C \rightarrow M_3@C_{80} \quad \Delta E_f \tag{1}$$

$$M_3 + C_{80} \rightarrow M_3@C_{80} \quad \Delta E_b \tag{2}$$

$$3M + C_{80} \rightarrow M_3@C_{80} \quad \Delta E_{encap} \tag{3}$$

$$3M \rightarrow M_3 \quad \Delta E_{cluster} \tag{4}$$

According to the calculation results (Fig. 1a–c), the values of the formation energy, the binding energy and the encapsulation energy become more negative from early lanthanide elements to late lanthanide elements. This trend is consistent with the decreasing order of the ionic radius of lanthanide elements. Therefore, the encapsulation of three lanthanide atoms with smaller sizes in I_h-C_{80} is more favorable in energy than the encapsulation of lanthanide atoms with larger sizes such as La and Nd, which is similar to the case of $M_3N@C_{80}$. Among all these compounds, $Tm_3@I_h$-C_{80} has the largest binding energy and encapsulation energy, indicating that the formation of $Tm_3@I_h$-C_{80} is more favorable than other $Ln_3@I_h$-C_{80} compounds. The binding energy has been used to interpret the stability of metallofullerenes.[36,57] For the lanthanide elements with a relatively small ionic radius such as Tm and Lu, their nitride clusterfullerenes $Ln_3N@C_{80}$ can be produced

Table 1 Relative energies (ΔE, in kcal mol^{-1}) and HOMO–LUMO gaps (H–L gap, in eV) of Tm_3C_{80} molecules calculated using PBE0 and PBE functionals (6-31G(d) and ECP58MWB basis sets are used for C and Tm atoms, respectively)

	PBE0		PBE	
Tm_3C_{80} (spiral number)	ΔE	H–L gap	ΔE	H–L gap
$Tm_3@I_h$ (31 924)-C_{80}	0.00	1.50[a]/2.70[b]	0.00	0.28[a]/1.43[b]
$Tm_3@D_{5h}$ (31 923)-C_{80}	14.08	0.28[a]/1.43[b]	13.32	0.28[a]/1.38[b]
$Tm_3@C_{2v}$ (31 922)-C_{80}	23.89	1.41[a]/1.59[b]	21.65	0.47[a]/0.59[b]
$Tm_3@C_{2v}$ (31 920)-C_{80}	37.40	0.95[a]/1.54[b]	34.54	0.09[a]/0.52[b]
$Tm_3@C_1$ (28 319)-C_{80}	41.63	1.19[a]/1.81[b]	36.56	0.32[a]/0.78[b]
$Tm_3@C_1$ (28 324)-C_{80}	42.91	1.56[a]/1.44[b]	38.98	0.52[a]/0.40[b]
$Tm_3@C_1$ (28 325)-C_{80}	31.18	1.34[a]/2.30[b]	29.62	0.27[a]/1.16[b]
$Tm_3@C_2$ (29 591)-C_{80}	36.42	1.40[a]/2.49[b]	35.20	0.24[a]/1.38[b]
$Tm_3@C_1$ (31 876)-C_{80}	38.68	1.60[a]/1.25[b]	34.04	0.59[a]/0.30[b]

[a] HOMO–LUMO gap for α spin orbitals. [b] HOMO–LUMO gap for β spin orbitals.

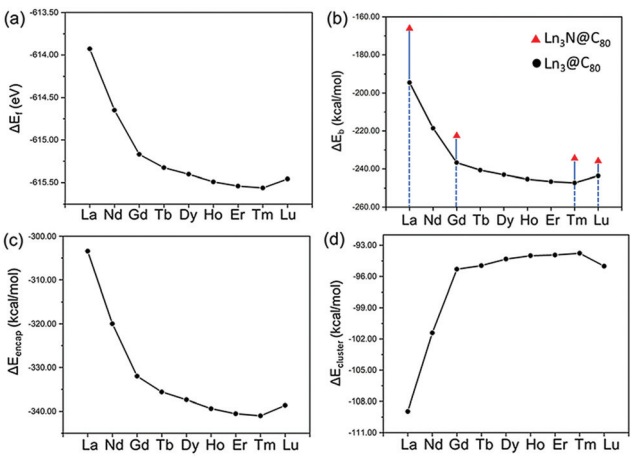

Fig. 1 The calculated (a) formation energies (ΔE_f), (b) binding energies (ΔE_b), and (c) encapsulation energies (ΔE_{encap}) of $Ln_3@I_h$-C_{80} (Ln = La, Nd, Gd, Tb, Dy, Ho, Er, Tm, Lu) and (d) the metal cluster formation energies ($\Delta E_{cluster}$) using the PBE functional.

in high yields experimentally. We calculated the binding energies of $Ln_3N@C_{80}$ (Ln = La, Gd, Tm, Lu) and compared them with that of $Ln_3@C_{80}$ (Fig. 1b). It is found that the binding energies of $Ln_3@I_h$-C_{80} compounds are larger than those of $Ln_3N@I_h$-C_{80}, implying that it is possible to obtain the metallofullerenes $Ln_3@I_h$-C_{80} in experiments.

Fig. 1d shows the metal cluster formation energy ($\Delta E_{cluster}$) for various lanthanide metals. It can be seen that $\Delta E_{cluster}$ becomes less negative on going from early lanthanide elements to late lanthanide elements. Although the cluster formation energy for Tm is the smallest among the metal elements, the encapsulation energy for $Tm_3@I_h$-C_{80} is the largest due to a strong interaction between the Tm_3 cluster and the I_h-C_{80} fullerene cage. Therefore, the interaction between the Ln_3 metal cluster and the fullerene cage contributes significantly to the driving force for the formation of $Ln_3@I_h$-C_{80} compounds.

3.2 Geometric structures of $Ln_3@I_h$-C_{80}

Fig. 2 and Fig. S1† show the optimized structures of $Ln_3@I_h$-C_{80} (Ln = La, Nd, Gd, Tb, Dy, Ho, Er, Tm, Lu) using PBE and PBE0 functionals, respectively. The encapsulated triangular metal cluster deforms the carbon cage and further causes symmetry reduction of the molecule. The structures of the Ln_3 cluster with the coordinated fullerene fragments are displayed in the figure for clarity. The Ln–Ln bond lengths of $Ln_3@I_h$-C_{80} in the ground states are summarized in Table 2. In most cases, the Ln–Ln distance is longer than that of a typical Ln–Ln single bond. When La_3 and Nd_3 clusters are encapsulated in I_h-C_{80}, each metal atom coordinates with a hexagonal carbon ring of the cage. The La or Nd metal atoms almost form an equilateral triangle with metal–metal distances of 3.274 Å–3.277 Å and 3.494 Å–3.499 Å in the case of La and Nd, respectively. As for the encapsulated Gd_3 and Tb_3 clusters, each metal atom is located near the junctions of three hexagons (penalene). In the case of $Dy_3@C_{80}$, three Dy atoms are non-equivalent. One Dy atom resides under a hexagonal ring, and the other two Dy atoms are located near the junctions of two hexagons (naphthalene). The Dy atoms in $Dy_3@C_{80}$ form an isosceles triangle with Dy–Dy distances of 3.437/3.470/3.470 Å, which are longer than the Dy–Dy distances in $Dy_3C_2@C_{80}$ (3.440/3.382/3.408 Å).[39] For the Ho_3, Er_3 and Tm_3 clusters, the metal atoms are situated at the junctions of one pentagon and two hexagons (acenaphthylene) as shown in the figure. In the situation of $Lu_3@C_{80}$, the three Lu atoms of the Lu_3 cluster show different characteristics. One Lu atom resides under a hexagon, and the other two Lu atoms are near the "naphthalene" and "acenaphthylene" fragments, respectively.

3.3 Electronic structure and bonding feature of $Ln_3@I_h$-C_{80}

The relative energies of $Ln_3@I_h$-C_{80} with different spin multiplicities are summarized in Table 2 and S3.† The calculations reveal that all the compounds have doublet ground states. The unpaired spin density distributions for the ground states of $Ln_3@I_h$-C_{80} compounds calculated using the PBE functional are shown in Fig. 3. The unpaired electron in $La_3@I_h$-C_{80} is mostly localized on the La_3 cluster, corresponding to a singly occupied three-center π bonding orbital. For the other $Ln_3@I_h$-C_{80} compounds, unpaired electron distributions both on the inner metal cluster moiety and on the fullerene cage can be

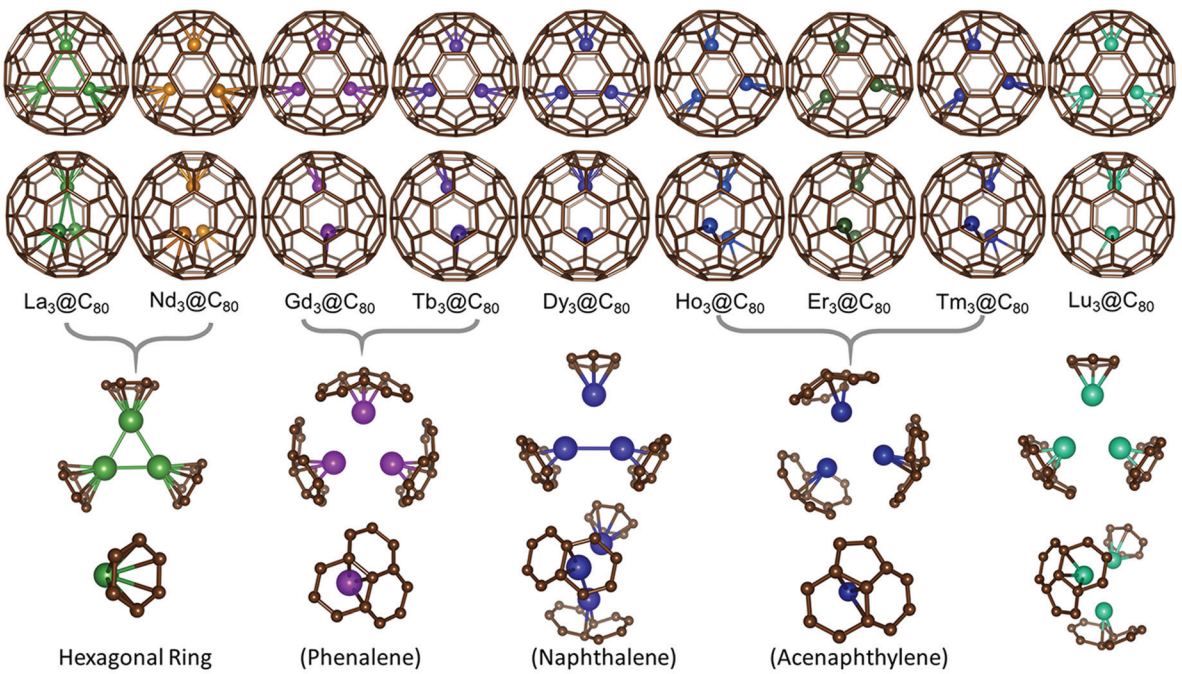

Fig. 2 The upper part shows the front view and side view of the optimized geometric structures of $Ln_3@I_h$-C_{80} (Ln = La, Nd, Gd, Tb, Dy, Ho, Er, Tm, Lu) using the PBE functional. The lower part shows the coordinated environments of the Ln_3 clusters inside the fullerene cage.

Table 2 Calculated relative energies (RE, in kcal mol^{-1}), Ln–Ln bond lengths (in Å), the Mayer bond order between the metal and the carbon atoms in $Ln_3@I_h$-C_{80} and spin population of the metal cluster

$Ln_3@C_{80}$ Metal atom	RE (in kcal mol^{-1})		Ln–Ln (in Å)				Mayer bond order				Spin population of the metal cluster
	Doublet	Quartet	1	2	3	Average	Ln_3	Ln(1)	Ln(2)	Ln(3)	
La	0	6.28	3.269	3.277	3.272	3.273	5.006	1.658	1.673	1.676	1.045
Nd	0	7.94	3.499	3.499	3.494	3.496	5.565	1.856	1.851	1.857	0.624
Gd	0	10.20	3.490	3.481	3.273	3.415	4.815	1.624	1.602	1.589	0.556
Tb	0	13.34	3.433	3.473	3.472	3.459	4.531	1.495	1.545	1.492	0.542
Dy	0	16.00	3.437	3.470	3.470	3.459	4.423	1.448	1.511	1.465	0.570
Ho	0	6.18	3.448	3.454	3.451	3.451	4.320	1.443	1.437	1.440	0.521
Er	0	21.53	3.437	3.465	3.434	3.445	4.054	1.361	1.375	1.318	0.697
Tm	0	23.32	3.443	3.466	3.457	3.455	4.219	1.425	1.402	1.392	0.576
Lu	0	28.47	3.319	3.568	3.575	3.487	4.263	1.314	1.311	1.638	0.636

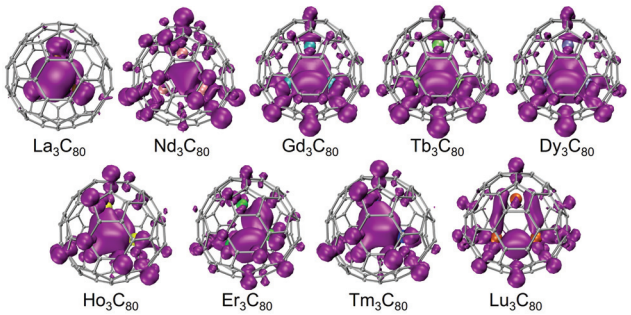

Fig. 3 The calculated spin density distributions of $Ln_3@I_h$-C_{80} (isovalue = 0.001).

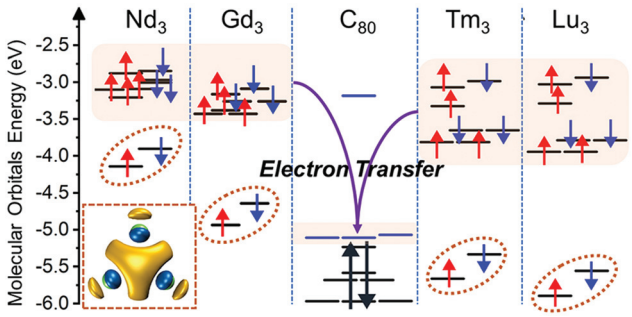

Fig. 4 The calculated canonical molecular orbital (CMO) energy level of I_h-C_{80} compared to those of Nd_3, Gd_3, Tm_3 and Lu_3 clusters in their ground states. The occupied and unoccupied molecular orbitals are denoted in black and blue lines, respectively. The CMOs corresponding to 3c-2e metal–metal bonding in Ln_3 clusters are encircled with orange dotted lines. As an example, the spatial distribution of the 3c-2e metal–metal bonding orbital for Nd_3 is shown in the bottom left corner of the figure.

observed. The calculated spin populations of the metal clusters are listed in Table 2. The La_3 cluster has a spin population of 1.045, while the spin population for other clusters is in the range of 0.5–0.7.

The neutral I_h-C_{80} molecule has almost degenerate LUMO/LUMO+1/LUMO+2 orbitals and a significantly large LUMO+2–LUMO+3 energy gap. Hence, the I_h-C_{80} cage prefers to accept six electrons to form a stable electronic configuration. Fig. 4 shows the energy levels of the canonical molecular orbitals (CMOs) for Ln_3 units and empty I_h-C_{80}. There are seven electrons that have close energy levels in the frontier molecular orbitals of the metal cluster. When the metal cluster is encapsulated into the I_h-C_{80} cage, six electrons are transferred to the LUMO/LUMO+1/LUMO+2 orbitals of I_h-C_{80}, and one unpaired electron is left on the metal cluster. The energy level of this singly occupied orbital is close to that of the LUMO+3 of I_h-C_{80}, resulting in a narrow HOMO–LUMO gap of $Ln_3@C_{80}$. The electronic configuration of $Ln_3@C_{80}$ can be described as $Ln_3^{6+}@C_{80}^{6-}$. The unpaired electron in $Ln_3@C_{80}$ occupies a molecular orbital with a relatively high energy. Consequently, the $Ln_3@C_{80}$ molecules have small ionization energies. Our DFT calculations reveal that the ionization energies of $Ln_3@C_{80}$ are in the range of 5.22–5.65 eV (Table S4†), which are much smaller than the calculated ionization energies of C_{60} (7.76 eV), C_{70} (7.56 eV) and $Ln_3N@C_{80}$ (around 6.79 eV). It has been reported that $Li@C_{60}$ can be oxidized to $Li@C_{60}^+$ and that it can form a variety of stable ionic compounds.[30–32] The calculated ionization energy of $Tm_3@C_{80}$ (5.50 eV) is smaller than that of $Li@C_{60}$ (5.73 eV). Therefore, it can be deduced that the $Tm_3@C_{80}$ molecule could be oxidized chemically to its cation $Tm_3@C_{80}^+$.

For bare Ln_3 clusters, there are molecular orbitals that correspond to three-center two-electron (3c-2e) bonding (encircled with orange dotted lines in Fig. 4). Because of the relatively low energy of these molecular orbitals, the 3c-2e bonding is preserved after the metal cluster is encapsulated in I_h-C_{80}. This is confirmed by examining the spatial distribution of molecular orbitals for $Ln_3@C_{80}$. As an example, the molecular orbital corresponding to 3c-2e bonding in $Tm_3@C_{80}$ is shown in Fig. 5a. ELF analysis also reveals that there exists three-center metal–metal bonding in $Tm_3@C_{80}$ (Fig. 5b). We found that the ELF for the encapsulated Tm_3 cluster is very different from the ELF for the bare Tm_3 cluster. In the case of the bare Tm_3 cluster, Tm–Tm bonding is observed at the edge rather than in the center of the cluster (Fig. 5b). Therefore, the bonding feature of the Tm_3 cluster is changed after being encaged in the sub-nanometer confined space of I_h-C_{80}. Moreover, our calculations reveal that the bonding feature of other Ln_3 clusters undergoes similar changes in I_h-C_{80}.

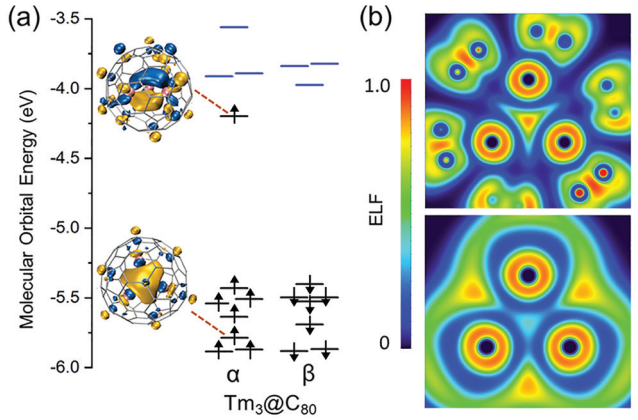

Fig. 5 (a) The molecular orbital energy diagram of the $Tm_3@I_h$-C_{80} molecule. The energy levels of the occupied and unoccupied CMOs are denoted in black and blue, respectively. The HOMO of $Tm_3@I_h$-C_{80} corresponds to a singly occupied π bonding orbital and the HOMO−5 corresponds to the 3c-2e metal−metal bonding orbital. (b) Color filled two-dimensional ELF maps of the metal cluster plane for $Tm_3@I_h$-C_{80} (upper part) and the bare Tm_3 cluster (lower part).

3.4 Chemical oxidation of $Tm_3@C_{80}$

As we discussed above, $Tm_3@C_{80}$ has large encapsulation and binding energies, implying that it is possible to obtain $Tm_3@C_{80}$ in experiments. Therefore, we performed arc-discharge synthesis of Tm-metallofullerenes. It has been reported that $AgSbF_6$ can be used to oxidize metallofullerenes into their cations.[58] Considering that $Tm_3@C_{80}$ has a small ionization energy, we treated the arc-discharge produced soot with $AgSbF_6$ in DCM. As a result, some Tm-metallofullerenes were oxidized into cations and they were solubilized in the solvent. Then, the solvent was evaporated and the resultant solid was redissolved in a mixture of toluene and acetonitrile (1 : 1). The mass spectrum of the solution (Fig. 6a) confirms that $Tm_3@C_{80}$ has been extracted from the raw soot. We ascribed the signal of $Tm_3@C_{80}$ to its cation, because no signal of $Tm_3@C_{80}$ was observed without using $AgSbF_6$.

The structure and electronic properties of the $Tm_3@C_{80}$ cation were studied using DFT calculations. Since the Tm_3 cluster may have different orientations inside the fullerene cage, we calculated the energies of different conformations of $Tm_3@C_{80}^+$. Their relative energies and geometrical parameters are listed in Table S6.† Fig. 6b shows the most stable structure of $Tm_3@C_{80}^+$ and the ELF distribution. The Tm–Tm distance in $Tm_3@C_{80}^+$ is in the range of 3.511–3.529 Å, which is longer than that in neutral $Tm_3@C_{80}$ (3.443 Å on average). Accordingly, the distance between the Tm atoms and the C_{80} cage gets shorter, leading to a stronger interaction between the Tm atoms and the fullerene cage. The total Mayer bond order between the Tm_3 cluster and the C_{80} cage increases from 4.219 to 4.777 after oxidation. As shown in Fig. 5a, the HOMO of $Tm_3@C_{80}$ corresponds to a singly occupied π bonding orbital. The removal of the electron in this orbital weakens the bonding between the Tm atoms. We examined the multi-center bond order (MCBO) for the Tm_3 cluster in $Tm_3@C_{80}$ and $Tm_3@C_{80}^+$. The MCBO index between the three Tm atoms in $Tm_3@C_{80}$ is 0.344, while that in $Tm_3@C_{80}^+$ is 0.331, indicat-

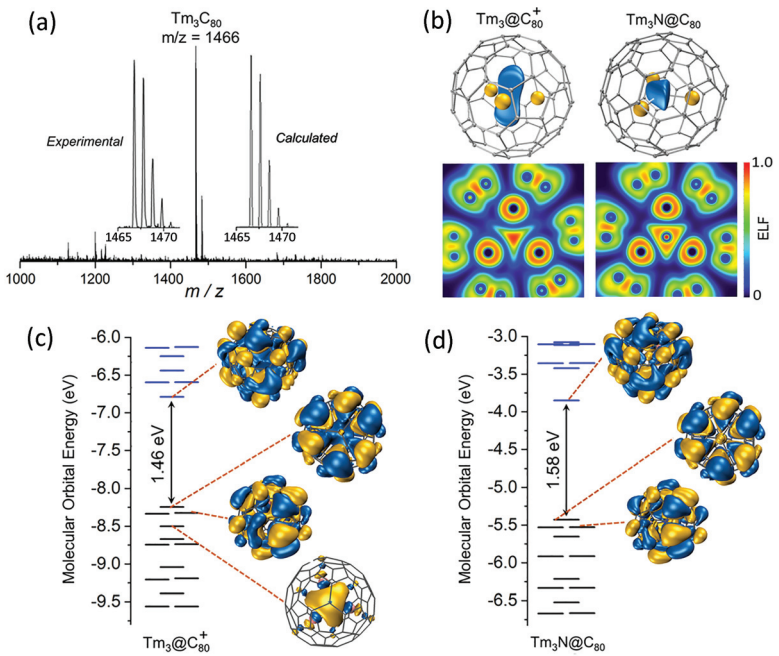

Fig. 6 (a) The experimental LDI-TOF mass spectrum of $Tm_3@C_{80}^+$ as well as the measured and calculated isotope distributions of the corresponding sample. (b) Three-dimensional ELF isosurface and color filled two-dimensional ELF maps of the metal cluster plane for the $Tm_3@I_h$-C_{80} cation (left) and $Tm_3N@I_h$-C_{80} molecule (right). (c and d) The molecular orbital energy diagrams of the $Tm_3@I_h$-C_{80} cation and $Tm_3N@I_h$-C_{80}. The energy levels of the occupied and unoccupied CMOs are denoted in black and blue, respectively.

ing that the three-center bond between Tm atoms in $Tm_3@C_{80}$ is stronger than that in $Tm_3@C_{80}^+$. Both the MCBO indices for the Tm_3 cluster in $Tm_3@C_{80}$ and $Tm_3@C_{80}^+$ are larger than that of the bare Tm_3 cluster (0.294). It should be noted that the average oxidation state of the Tm atom increases from +2 to +7/3 after oxidation of $Tm_3@C_{80}$. This change leads to a stronger electrostatic repulsion between the Tm ions inside the fullerene cage. In this situation, the cation $Tm_3@C_{80}^+$ can still survive because the 3c-2e bonding between the Tm ions significantly compensates for the repulsion effect. As shown in Fig. 6b, the ELF distribution of $Tm_3@C_{80}^+$ reveals that there exists three-center bonding between the Tm ions. Fig. 6c shows the molecular orbitals of $Tm_3@C_{80}^+$. It can be seen that the molecular orbital HOMO−3 corresponds to a three-center σ bond.

It is known that $Tm_3N@C_{80}$ is a clusterfullerene with high stability. In this study, we found that both the molecular geometry and the electronic structure of $Tm_3@C_{80}^+$ resemble that of $Tm_3N@C_{80}$. The Tm–Tm distance in $Tm_3@C_{80}^+$ (3.511–3.529 Å) is very close to that in $Tm_3N@C_{80}$ (around 3.55 Å). Meanwhile, the ELF distribution of $Tm_3@C_{80}^+$ is also similar to that of $Tm_3N@C_{80}$ (Fig. 6b). In the case of $Tm_3N@C_{80}$, the formal charge of the Tm atom is +3, and there is a strong electrostatic repulsion between the Tm^{3+} ions. The central N^{3-} ion serves as a mediator and it reduces the repulsion between the Tm^{3+} ions. In the case of $Tm_3@C_{80}^+$, the three-center σ bond plays a similar role to the N^{3-} ion in $Tm_3N@C_{80}$. As a result, three Tm ions can be accommodated inside the C_{80} cage without a nonmetal mediator. Therefore, the three-center σ bond is a critical factor that stabilizes the tri-metallofullerene cation. Furthermore, we found that $Tm_3@C_{80}^+$ and $Tm_3N@C_{80}$ have similar Frontier molecular orbitals. The energy diagrams and spatial distributions of the frontier molecular orbitals of $Tm_3@C_{80}^+$ and $Tm_3N@C_{80}$ are shown in Fig. 6c and d. It can be seen that the molecular orbitals including the LUMO, HOMO and HOMO−1 for $Tm_3@C_{80}^+$ and $Tm_3N@C_{80}$ are very similar in shape. Meanwhile, the calculated HOMO–LUMO gap of $Tm_3@C_{80}^+$ (1.46 eV) using the PBE functional is close to that of $Tm_3N@C_{80}$ (1.58 eV). Among all the reported metallofullerenes, $M_3N@C_{80}$ is a kind of metallofullerenes that have large HOMO–LUMO gaps. DFT calculations in this work reveal that $Tm_3@C_{80}^+$ also has a large HOMO–LUMO gap, implying that this cation has high stability. It should be noted that the neutral $Tm_3@C_{80}$ has a rather small HOMO–LUMO gap (0.28 eV), indicating that it is a chemically reactive molecule. Because $Tm_3@C_{80}^+$ has a much larger HOMO–LUMO gap, the chemical stability of $Tm_3@C_{80}$ can be enhanced greatly upon oxidation. The change in the HOMO–LUMO gap explains the following facts: (1) the neutral $Tm_3@C_{80}$ is not observed in the extract of raw soot by using conventional fullerene solvents such as toluene and xylene; (2) $Tm_3@C_{80}$ can be chemically oxidized to a stable cation $Tm_3@C_{80}^+$. Besides $Tm_3@C_{80}^+$, tri-metallofullerene cations containing other metals such as $Er_3@C_{80}^+$ and $Dy_3@C_{80}^+$ can also be obtained through a similar oxidation method (Fig. S2†).

4 Conclusions

DFT calculations demonstrated that tri-metallofullerenes $Ln_3@C_{80}$ are thermodynamically stable molecules. The binding energy of $Ln_3@C_{80}$ is larger than that of the nitride clusterfullerene $Ln_3N@C_{80}$, revealing that encapsulation of a Ln_3 cluster in C_{80} is favorable in energy. DFT calculations also revealed that $Ln_3@C_{80}$ has the smallest ionization energy among the metallofullerene molecules reported so far. We used $AgSbF_6$ to oxidize the arc-discharge-produced soot containing $Tm_3@C_{80}$ and obtained the cation $Tm_3@C_{80}^+$. We found that both the molecular geometry and the electronic structure of $Tm_3@C_{80}^+$ resemble that of $Tm_3N@C_{80}$. In particular, both of them have large HOMO–LUMO gaps, implying that $Tm_3@C_{80}^+$ has high stability as $Tm_3N@C_{80}$ does. There is a three-center two-electron σ bond in the center of the Tm_3 cluster in $Tm_3@C_{80}^+$. This special metal–metal bond compensates for the electrostatic repulsion between the Tm ions and thus greatly stabilizes the cation $Tm_3@C_{80}^+$. The metallofullerene cations $Ln_3@C_{80}^+$ can be used as building blocks to construct a variety of novel ionic compounds $Ln_3@C_{80}^+X^-$ in future studies.

Conflicts of interest

There are no conflicts to declare.

Acknowledgements

We are grateful for the support from the Outstanding Innovative Talents Cultivation Funded Programs 2021 of Renmin University of China, the Beijing Municipal Natural Science Foundation (grant no. 2212030), and the National Natural Science Foundation of China (grant no. 22175199). Resources supporting this work were provided by the Public Computing Cloud Platform of Renmin University of China.

Notes and references

1 A. A. Popov, S. Yang and L. Dunsch, Endohedral fullerenes, *Chem. Rev.*, 2013, **113**, 5989–6113.
2 H. Cong, B. Yu, T. Akasaka and X. Lu, Endohedral metallofullerenes: An unconventional core–shell coordination union, *Coord. Chem. Rev.*, 2013, **257**, 2880–2898.
3 S. Yang, T. Wei and F. Jin, When metal clusters meet carbon cages: endohedral clusterfullerenes, *Chem. Soc. Rev.*, 2017, **46**, 5005–5058.
4 M. N. Chaur, F. Melin, A. L. Ortiz and L. Echegoyen, Chemical, electrochemical, and structural properties of endohedral metallofullerenes, *Angew. Chem., Int. Ed.*, 2009, **48**, 7514–7538.
5 T. Wang and C. Wang, Endohedral Metallofullerenes Based on Spherical I_h-C_{80} Cage: Molecular Structures and Paramagnetic Properties, *Acc. Chem. Res.*, 2014, **47**, 450–458.

6 X. Zhang, Y. Wang, R. Morales-Martínez, J. Zhong, C. de Graaf, A. Rodríguez-Fortea, J. M. Poblet, L. Echegoyen, L. Feng and N. Chen, $U_2@I_h(7)$-C_{80}: Crystallographic Characterization of a Long-Sought Dimetallic Actinide Endohedral Fullerene, *J. Am. Chem. Soc.*, 2018, **140**, 3907–3915.

7 X. Li, Y. Roselló, Y.-R. Yao, J. Zhuang, X. Zhang, A. Rodríguez-Fortea, C. de Graaf, L. Echegoyen, J. M. Poblet and N. Chen, $U_2N@I_h(7)$-C_{80}: Fullerene Cage Encapsulating an Unsymmetrical U (IV) = N = U (V) Cluster, *Chem. Sci.*, 2021, **12**, 282–292.

8 X. Zhang, W. Li, L. Feng, X. Chen, A. Hansen, S. Grimme, S. Fortier, D.-C. Sergentu, T. J. Duignan, J. Autschbach, *et al.*, A diuranium carbide cluster stabilized inside a C_{80} fullerene cage, *Nat. Commun.*, 2018, **9**, 1–8.

9 J. Zhuang, R. Morales-Martínez, J. Zhang, Y. Wang, Y.-R. Yao, C. Pei, A. Rodríguez-Fortea, S. Wang, L. Echegoyen, C. de Graaf, *et al.*, Characterization of a strong covalent Th^{3+}-Th^{3+} bond inside an $I_h(7)$-C_{80} fullerene cage, *Nat. Commun.*, 2021, **12**, 1–8.

10 K. Junghans, M. Rosenkranz and A. A. Popov, $Sc_3CH@C_{80}$: selective ^{13}C enrichment of the central carbon atom, *Chem. Commun.*, 2016, **52**, 6561–6564.

11 C. Zhao, K. Tan, M. Nie, Y. Lu, J. Zhang, C. Wang, X. Lu and T. Wang, Scandium Tetrahedron Supported by H Anion and CN Pentaanion inside Fullerene C_{80}, *Inorg. Chem.*, 2020, **59**, 8284–8290.

12 C. Fuertes-Espinosa, A. Gómez-Torres, R. Morales-Martínez, A. Rodríguez-Fortea, C. García-Simón, F. Gándara, I. Imaz, J. Juanhuix, D. Maspoch, J. M. Poblet, *et al.*, Purification of Uranium-based Endohedral Metallofullerenes (EMFs) by Selective Supramolecular Encapsulation and Release, *Angew. Chem., Int. Ed.*, 2018, **57**, 11294–11299.

13 Z. Wei, L. Yang, J. Ji, Q. Hou, L. Li and P. Jin, Undiscovered Effect of C↔N Interchange Inside the Metal Carbonitride Clusterfullerenes: A Density Functional Theory Investigation, *Inorg. Chem.*, 2020, **59**, 6518–6527.

14 T. Suzuki, Y. Maruyama, T. Kato, K. Kikuchi, Y. Nakao, Y. Achiba, K. Kobayashi and S. Nagase, Electrochemistry and ab initio study of the dimetallofullerene $La_2@C_{80}$, *Angew. Chem., Int. Ed. Engl.*, 1995, **34**, 1094–1096.

15 Z. Wang, R. Kitaura and H. Shinohara, Metal-dependent stability of pristine and functionalized unconventional dimetallofullerene $M_2@I_h$-C_{80}, *J. Phys. Chem. C*, 2014, **118**, 13953–13958.

16 F. Liu, L. Spree, D. S. Krylov, G. Velkos, S. M. Avdoshenko and A. A. Popov, Single-electron lanthanide-lanthanide bonds inside fullerenes toward robust redox-active molecular magnets, *Acc. Chem. Res.*, 2019, **52**, 2981–2993.

17 Y. Jiang, Z. Li, J. Zhang and Z. Wang, Endohedral metallofullerene $M_2@C_{80}$: A new class of magnetic superhalogen, *J. Phys. Chem. C*, 2019, **124**, 2131–2136.

18 F. Liu, G. Velkos, D. S. Krylov, L. Spree, M. Zalibera, R. Ray, N. A. Samoylova, C.-H. Chen, M. Rosenkranz, S. Schiemenz, *et al.*, Air-stable redox-active nanomagnets with lanthanide spins radical-bridged by a metal–metal bond, *Nat. Commun.*, 2019, **10**, 1–11.

19 L. Dunsch and S. Yang, Metal nitride cluster fullerenes: their current state and future prospects, *Small*, 2007, **3**, 1298–1320.

20 Y. Lian, Z. Shi, X. Zhou and Z. Gu, Different extraction Behaviors between divalent and trivalent endohedral metallofullerenes, *Chem. Mater.*, 2004, **16**, 1704–1714.

21 A. A. Popov, L. Zhang and L. Dunsch, A pseudoatom in a cage: Trimetallofullerene $Y_3@C_{80}$ mimics $Y_3N@C_{80}$ with nitrogen substituted by a pseudoatom, *ACS Nano*, 2010, **4**, 795–802.

22 W. Xu, L. Feng, M. Calvaresi, J. Liu, Y. Liu, B. Niu, Z. Shi, Y. Lian and F. Zerbetto, An Experimentally Observed Trimetallofullerene $Sm_3@I_h$-C_{80}: Encapsulation of Three Metal Atoms in a Cage without a Nonmetallic Mediator, *J. Am. Chem. Soc.*, 2013, **135**, 4187–4190.

23 N. Tagmatarchis, E. Aslanis, K. Prassides and H. Shinohara, Mono-, di- and trierbium endohedral metallofullerenes: Production, separation, isolation, and spectroscopic study, *Chem. Mater.*, 2001, **13**, 2374–2379.

24 S. Yang and L. Dunsch, Di-and tridysprosium endohedral metallofullerenes with cages from C_{94} to C_{100}, *Angew. Chem., Int. Ed.*, 2006, **45**, 1299–1302.

25 Y.-J. Guo, H. Zheng, T. Yang, S. Nagase and X. Zhao, Theoretical Insight into the Ambiguous Endohedral Metallofullerene Er_3C_{74}: Covalent Interactions among Three Lanthanide Atoms, *Inorg. Chem.*, 2015, **54**, 8066–8076.

26 Y. Wang, L. Ma, L. Mu, J. Ren and X. Kong, A systematic study on the generation of multimetallic lanthanide fullerene ions by laser ablation mass spectrometry, *Rapid Commun. Mass Spectrom.*, 2018, **32**, 1396–1402.

27 Y. Wang, J. Ren, L. Mu and X. Kong, Metallofullerene ions of $Lu_nC_{2m}^+$ ($1\leq n\leq 9$, $50\leq 2m\leq 198$) generated by laser ablation of graphene/$LuCl_3$, *Int. J. Mass Spectrom.*, 2017, **422**, 105–110.

28 L. Mu, S. Yang, R. Feng and X. Kong, Encapsulation of Platinum in Fullerenes: Is That Possible?, *Inorg. Chem.*, 2017, **56**, 6035–6038.

29 X. Kong and X. Bao, Formation of endohedral metallofullerene (EMF) ions of (M = La, Y, $n\leq 6$, $50\leq 2m\leq 194$) in the laser ablation process with graphene as precursor, *Rapid Commun. Mass Spectrom.*, 2017, **31**, 865–872.

30 S. Aoyagi, E. Nishibori, H. Sawa, K. Sugimoto, M. Takata, Y. Miyata, R. Kitaura, H. Shinohara, H. Okada, T. Sakai, *et al.*, A layered ionic crystal of polar $Li@C_{60}$ superatoms, *Nat. Chem.*, 2010, **2**, 678–683.

31 S. Aoyagi, Y. Sado, E. Nishibori, H. Sawa, H. Okada, H. Tobita, Y. Kasama, R. Kitaura and H. Shinohara, Rock-Salt-Type Crystal of Thermally Contracted C_{60} with Encapsulated Lithium Cation, *Angew. Chem., Int. Ed.*, 2012, **51**, 3377–3381.

32 H. Okada, T. Komuro, T. Sakai, Y. Matsuo, Y. Ono, K. Omote, K. Yokoo, K. Kawachi, Y. Kasama, S. Ono, *et al.*, Preparation of endohedral fullerene containing lithium

($Li@C_{60}$) and isolation as pure hexafluorophosphate salt ($[Li^+@C_{60}][PF_6^-]$), *RSC Adv.*, 2012, **2**, 10624–10631.
33 H. Okada and Y. Matsuo, Anion exchange of $Li^+@C_{60}$ salt for improved solubility, *Fullerenes, Nanotubes, Carbon Nanostruct.*, 2014, **22**, 262–268.
34 J. P. Perdew, K. Burke and M. Ernzerhof, Generalized gradient approximation made simple, *Phys. Rev. Lett.*, 1996, **77**, 3865.
35 C. Adamo and V. Barone, Toward reliable density functional methods without adjustable parameters: The PBE0 model, *J. Chem. Phys.*, 1999, **110**, 6158–6170.
36 A. A. Popov and L. Dunsch, Structure, Stability, and Cluster-Cage Interactions in Nitride Clusterfullerenes $M_3N@C_{2n}$ (M = Sc, Y; 2n = 68–98): a Density Functional Theory Study, *J. Am. Chem. Soc.*, 2007, **129**, 11835–11849.
37 Q. Meng, L. Abella, W. Yang, Y.-R. Yao, X. Liu, J. Zhuang, X. Li, L. Echegoyen, J. Autschbach and N. Chen, $UCN@C_s(6)$-C_{82}: An Encapsulated Triangular UCN Cluster with Ambiguous U Oxidation State [U (III) versus U (I)], *J. Am. Chem. Soc.*, 2021, **143**, 16226–16234.
38 X. Ge, X. Dai, H. Zhou, Z. Yang and R. Zhou, Stabilization of Open-Shell Single Bonds within Endohedral Metallofullerene, *Inorg. Chem.*, 2020, **59**, 3606–3618.
39 F. Jin, J. Xin, R. Guan, X.-M. Xie, M. Chen, Q. Zhang, A. A. Popov, S.-Y. Xie and S. Yang, Stabilizing a three-center single-electron metal–metal bond in a fullerene cage, *Chem. Sci.*, 2021, **12**, 6890–6895.
40 P. C. Hariharan and J. A. Pople, The Influence of Polarization Functions on Molecular Orbital Hydrogenation Energies, *Theor. Chim. Acta*, 1973, **28**, 213–222.
41 R. Krishnan, J. S. Binkley, R. Seeger and J. A. Pople, Self-Consistent Molecular Orbital Methods. XX. A Basis Set for Correlated Wave Functions, *J. Chem. Phys.*, 1980, **72**, 650–654.
42 I. Mayer, Charge, Bond Order and Valence in the Ab Initio SCF Theory, *Chem. Phys. Lett.*, 1983, **97**, 270–274.
43 M. Giambiagi, M. S. de Giambiagi and K. C. Mundim, Definition of a multicenter bond index, *Struct. Chem.*, 1990, **1**, 423–427.
44 A. Savin, R. Nesper, S. Wengert and T. F. Fässler, ELF: The electron localization function, *Angew. Chem., Int. Ed. Engl.*, 1997, **36**, 1808–1832.
45 T. Lu and F. Chen, Multiwfn: a multifunctional wavefunction analyzer, *J. Comput. Chem.*, 2012, **33**, 580–592.
46 M. J. Frisch, G. W. Trucks, H. B. Schlegel, G. E. Scuseria, M. A. Robb, J. R. Cheeseman, G. Scalmani, V. Barone, G. A. Petersson, H. Nakatsuji, X. Li, M. Caricato, A. V. Marenich, J. Bloino, B. G. Janesko, R. Gomperts, B. Mennucci, H. P. Hratchian, J. V. Ortiz, A. F. Izmaylov, J. L. Sonnenberg, D. Williams-Young, F. Ding, F. Lipparini, F. Egidi, J. Goings, B. Peng, A. Petrone, T. Henderson, D. Ranasinghe, V. G. Zakrzewski, J. Gao, N. Rega, G. Zheng, W. Liang, M. Hada, M. Ehara, K. Toyota, R. Fukuda, J. Hasegawa, M. Ishida, T. Nakajima, Y. Honda, O. Kitao, H. Nakai, T. Vreven, K. Throssell, J. A. Montgomery Jr., J. E. Peralta, F. Ogliaro, M. J. Bearpark, J. J. Heyd, E. N. Brothers, K. N. Kudin, V. N. Staroverov, T. A. Keith, R. Kobayashi, J. Normand, K. Raghavachari, A. P. Ren-dell, J. C. Burant, S. S. Iyengar, J. Tomasi, M. Cossi, J. M. Millam, M. Klene, C. Adamo, R. Cammi, J. W. Ochterski, R. L. Martin, K. Morokuma, O. Farkas, J. B. Foresman and D. J. Fox, *Gaussian 16 Revision A.03*, Gaussian Inc, Wallingford CT, 2016.
47 W. Humphrey, A. Dalke, K. Schulten, *et al.*, VMD: Visual Molecular Dynamics, *J. Mol. Graphics*, 1996, **14**, 33–38.
48 Y. Iiduka, T. Wakahara, T. Nakahodo, T. Tsuchiya, A. Sakuraba, Y. Maeda, T. Akasaka, K. Yoza, E. Horn, T. Kato, *et al.*, Structural determination of metallofullerene Sc_3C_{82} revisited: a surprising finding, *J. Am. Chem. Soc.*, 2005, **127**, 12500–12501.
49 P. Yu, W. Shen, L. Bao, C. Pan, Z. Slanina and X. Lu, Trapping an unprecedented Ti_3C_3 unit inside the icosahedral C_{80} fullerene: a crystallographic survey, *Chem. Sci.*, 2019, **10**, 10925–10930.
50 T. Zuo, M. M. Olmstead, C. M. Beavers, A. L. Balch, G. Wang, G. T. Yee, C. Shu, L. Xu, B. Elliott, L. Echegoyen, *et al.*, Preparation and Structural Characterization of the I_h and the D_{5h} Isomers of the Endohedral Fullerenes $Tm_3N@C_{80}$: Icosahedral C_{80} Cage Encapsulation of a Trimetallic Nitride Magnetic Cluster with Three Uncoupled Tm^{3+} Ions, *Inorg. Chem.*, 2008, **47**, 5234–5244.
51 P. Jin, C. Tang and Z. Chen, Carbon atoms trapped in cages: metal carbide clusterfullerenes, *Coord. Chem. Rev.*, 2014, **270**, 89–111.
52 B. Cao, M. Hasegawa, K. Okada, T. Tomiyama, T. Okazaki, K. Suenaga and H. Shinohara, EELS and ^{13}C NMR characterization of pure $Ti_2@C_{80}$ metallofullerene, *J. Am. Chem. Soc.*, 2001, **123**, 9679–9680.
53 H. Yang, C. Lu, Z. Liu, H. Jin, Y. Che, M. M. Olmstead and A. L. Balch, Detection of a Family of Gadolinium-Containing Endohedral Fullerenes and the Isolation and Crystallographic Characterization of One Member as a Metal-Carbide Encapsulated inside a Large Fullerene Cage, *J. Am. Chem. Soc.*, 2008, **130**, 17296–17300.
54 J. Zhang, T. Fuhrer, W. Fu, J. Ge, D. W. Bearden, J. Dallas, J. Duchamp, K. Walker, H. Champion, H. Azurmendi, *et al.*, Nanoscale fullerene compression of an yttrium carbide cluster, *J. Am. Chem. Soc.*, 2012, **134**, 8487–8493.
55 J. M. Campanera, C. Bo and J. M. Poblet, General rule for the stabilization of fullerene cages encapsulating trimetallic nitride templates, *Angew. Chem., Int. Ed.*, 2005, **44**, 7230–7233.
56 M. Krause and L. Dunsch, Gadolinium nitride Gd_3N in carbon cages: the influence of cluster size and bond strength, *Angew. Chem., Int. Ed.*, 2005, **44**, 1557–1560.
57 L. Bao, Y. Li, P. Yu, W. Shen, P. Jin and X. Lu, Preferential Formation of Mono-Metallofullerenes Governed by the Encapsulation Energy of the Metal Elements: A Case Study on $Eu@C_{2n}$ (2n = 74–84) Revealing a General Rule, *Angew. Chem., Int. Ed.*, 2020, **59**, 5259–5262.
58 R. D. Bolskar and J. M. Alford, Chemical oxidation of endohedral metallofullerenes: identification and separation of distinct classes, *Chem. Commun.*, 2003, 1292–1293.